

Crystal Plasticity Analysis of Texture Evolution of Pure Aluminum During Processing by a New Severe Plastic Deformation Technique



ALI KHAJEZADE, MOHAMMAD HABIBI PARSA, and HAMED MIRZADEH

Texture evolution in a newly developed severe plastic deformation technique, named multi-axial incremental forging and shearing (MAIFS), was studied applying the visco-plastic self-consistent crystal plasticity formulation by consideration of macroscopic deformation history. The simulated texture evolutions revealed that although shear-like texture had developed by the MAIFS process, texture components rotated around normal to mid-plane section. This could be ascribed to the complex deformation history that naturally develops during processing by the MAIFS process. The increased complexity of the deformation history in the MAIFS process, compared to the techniques that are solely based on the simple shear deformation, causes more activated slip planes, which in turn can result in an enhanced grain refinement ability of this processing technique.

DOI: 10.1007/s11661-015-3227-3

© The Minerals, Metals & Materials Society and ASM International 2015

I. INTRODUCTION

ULTRA-FINE grained (UFG) materials have gained a lot of attention because of their excellent mechanical and physical properties and the possibility for achieving high-strain rate superplasticity.^[1] Broad ranges of techniques have been invented to produce UFG materials. Severe plastic deformation (SPD) methods may be mentioned as one of the most effective bulk deformation processes that can produce UFG materials. In these processes, the material experiences a large amount of strain, while returning to the approximate initial geometry at the end of deformation.^[2] By today's definition, SPD of bulk materials was first introduced by the invention of equal channel angular extrusion (ECAE).^[3] In ECAE, one metallic sample experiences large shear strain by pressing through an angular channel with the same inlet and outlet channel size. Numbers of versatile methods have been introduced to impose SPD on the material for more effective and flexible microstructural refinement.^[4] High pressure

torsion (HPT), accumulative roll bonding (ARB), multi-directional forging (MDF), and twist extrusion (TE) are popular severe SPD techniques, while there are lots of other techniques that are either derivative or just the innovative combinations of these techniques.^[4]

In HPT technique, large shear strain could be imposed on a disk in the presence of high hydrostatic pressure to prevent the initiation and growth of cracks in the material. In ARB, the stacked metallic sheets are rolled by minimum 50 pct reduction thickness. This process is continued by cutting, stacking of rolled sheets, and repetition of rolling until the desired amount of strain is reached. In MDF technique, high strain could be imposed by plane strain forging of rectangular cubic specimen in successive different axes. TE is the technique that the large strain is imposed by the simultaneous twisting and extrusion.

Despite the simplicity of required instruments for SPD processes, the mechanical behavior and the microstructural evolution in the deformed material are very complex. This issue can be best described by crystal plasticity analysis, where microstructural behavior of the material can be related to the macroscopic deformation. The importance of crystal plasticity analysis in SPD processes can be traced back by extensive analysis of this kind on ECAE process. Gholinia *et al.*^[5] used experimental deformation gradient examinations during ECAE and a simple full constraint Taylor model to predict texture evolution in pure Aluminum subjected to SPD. They showed that components of deformation other than simple shear change the final texture, effectively. This work may be the first one emphasizing on the importance of considering the deformation components and deformation history for texture and microstructural evolutions in ECAE process.

Tóth *et al.*^[6,7] proposed an analytical new flow field to model deformation history and simulated texture evolution by visco-plastic self-consistent method (VPSC).^[8] Deng

ALI KHAJEZADE, MS Student, is with the School of Metallurgy and Materials Engineering, College of Engineering, University of Tehran, P.O. Box 11155-4563, Tehran, Iran. MOHAMMAD HABIBI PARSA, Professor, is with the School of Metallurgy and Materials Engineering, College of Engineering, University of Tehran, and also with the Center of Excellence for High Performance Materials, School of Metallurgy and Materials Engineering, University of Tehran, and also with the Advanced Metal Forming and Thermomechanical Processing Laboratory, School of Metallurgy and Materials Engineering, University of Tehran. Contact e-mail: mhparsa@ut.ac.ir HAMED MIRZADEH, Assistant Professor, is with the School of Metallurgy and Materials Engineering, College of Engineering, University of Tehran, and also with the Advanced Metal Forming and Thermomechanical Processing Laboratory, School of Metallurgy and Materials Engineering, University of Tehran.

Manuscript submitted October 23, 2014.

Article published online November 13, 2015

et al.^[9], inspired from this idea, developed an analytical model for non-equal channel angular extrusion (NECAE is the same technique as ECAE with the difference of having smaller outlet channel in comparison to inlet channel) and regenerated the final texture by using of this model. Beyerlein *et al.*^[10] used VPSC method to investigate different process and material models for simulating ECAE of FCC polycrystals. Ferrasse *et al.*^[11] also used crystal plasticity analysis to understand the effect of ECAE routes on texture evolution. Li *et al.*^[12] emphasized on the effect of deformation history and commented on the suggested ECAE crystal plasticity analysis in the literature. They mentioned that deformation history may not be chosen correctly in previous studies and stated that negative shear should be selected for simulation of ECAE for good correspondence of modeling results with experiments. Of course, it is still possible to correctly reproduce the final texture by considering positive shear accompanied by complex rotation of calculated texture. A better texture evolution in ECAE process was accomplished by Li *et al.*^[13] considering coupling of finite element simulation and crystal plasticity. Texture formation analysis using three-dimensional finite difference method considering deformation history for a different crystal plasticity analysis was conducted by Alexandrov *et al.*,^[14] and the results were compared with experimental results for different routes of ECAE. Kalidindi *et al.*^[15] analyzed microscopic strain inhomogeneity by finite element crystal plasticity analysis. They simulated inhomogeneity of deformation in ECAE by simulation of different ECAE routes with different die parameters. This was inspired by the work of Tóth *et al.*,^[7] where inhomogeneity was modeled by different flow lines. Strain inhomogeneity and deformation history issue are the main subject of many studies in crystal plasticity (*e.g.*, Reference 16 through 18). There are also some numerical and theoretical frameworks on the crystal plasticity analysis of crystal structures other than FCC (*e.g.*, Reference 19 through 23).

Recently, a new SPD method had been introduced by Montazeri-Pour *et al.*^[24] named multi-axial incremental forging and shearing (MAIFS). This method can be categorized as a subset to ECAE. The difference between this method and ECAE is that material is extruded through the channel by two or more shear punches in place of one pressing punch. Figure 1 shows a schematic representation of different steps for one pass of the MAIFS process. This kind of process gives specimen the chance to experience more complex deformation history and one can impose an extra shear component in different shear planes.

The current work is going to investigate the texture evolution in the MAIFS process by the VPSC proposed by Lebensohn *et al.*^[8] It should be noted that texture analysis in this kind of process is critical because of the intrinsic inhomogeneity of the process.

II. METHODOLOGY

A. Experiment

Deformation history in the MAIFS process is intrinsically complex and inhomogeneous. The inhomogeneity

arises from the process can be qualitatively shown by metallographic examinations. The flow lines and material deformation path can be traced by metallographic investigations. Thus, it becomes possible to understand how every material's point moved compared to its adjacent and this qualitatively shows the degree of inhomogeneity during deformation. $20 \times 20 \times 40 \text{ mm}^3$ prepared aluminum specimens were subjected to SPD by the MAIFS process. The mid-plane section was cut and macro-etched by 4M Keller's reagent.^[25]

B. Simulation

For direct crystal plasticity simulation, an essential point in microstructural simulation is the calculation of deformation history. Gholinia *et al.*^[5] used experimental practice to determine deformation history in ECAE process. In the present work, the finite element simulation software, ABAQUS, was used to determine the deformation history. To simulate the MAIFS process, two-dimensional model discretized with plane strain element was used. The mesh size was chosen according to mesh sensitivity analysis. The result of this analysis is summarized in Figure 2. The analysis involves in tracing the amount of reaction force on the first shear punch *versus* the mesh size. The mesh size of 1 mm is optimal due to the fact that reduction in mesh size just increases the cost of calculation without any significant effect on the result. Schematic representation of model is shown in Figure 3.

As can be seen, three rigid punches with width of 10 mm and a $40 \times 40 \text{ mm}^2$ rigid die were used. One $20 \times 40 \text{ mm}^2$ deformable specimen with mechanical properties obtained from stress-strain curve shown in Figure 4 was used as the modeling material. The stress-strain curve used here was obtained from the torsion test by consideration of the equivalent stress and strain based on the von Mises criterion^[26] to be presentable for processes involving high level of strain. The flow curve obtained from torsion test is a better representation of materials behavior in comparison to tensile or compression test, where reaching high number of strain is very limited. Elastic properties used in the simulation are summarized in Table I.

The process was simulated in three explicit steps to trace any possible dynamic effects. Each step is related to the relevant punch movement. Mass scaling was used to reduce computational costs. Friction coefficient of 0.12 (sliding friction) was used to model every surface contact in this simulation, and the surface-to-surface contact was defined for each contact pair.

After simulation, deformation history can be represented by strain rate tensor which can be approximated as follows:

$$\dot{\mathbf{E}}_{ij} = \frac{E_{ij}^2 - E_{ij}^1}{\Delta t}, \quad [1]$$

where E_{ij}^2 and E_{ij}^1 are strain tensor components in two successive time increments of Δt . The strain history can be directly extracted from ABAQUS database by asking the proper history output. For this investigation, strain

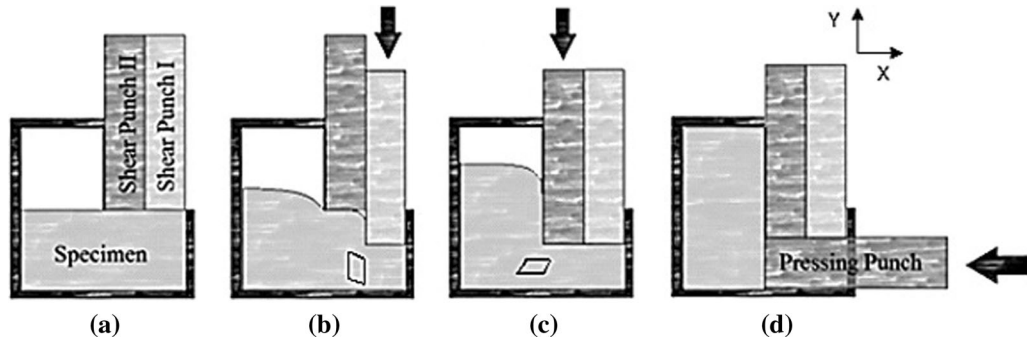


Fig. 1—Three steps of the MAIFS process (a) undeformed state, (b) first shearing and compression, (c) second shearing and compression, (d) final non-equal channel angular extrusion. Shear states were also shown between shear punches and final non-equal channel angular extrusion.

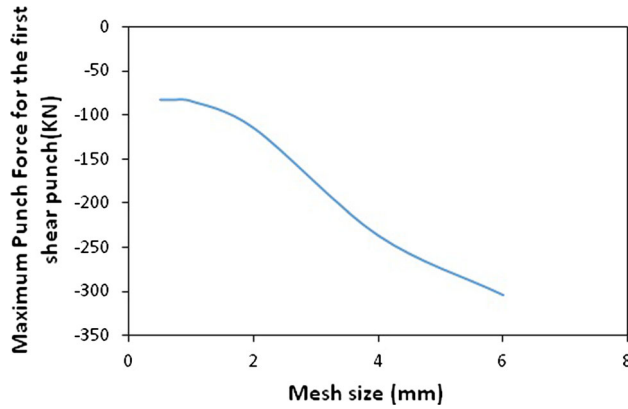


Fig. 2—The result of mesh sensitivity analysis.

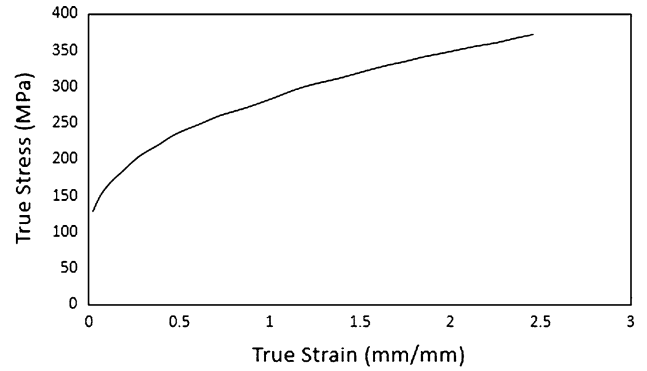


Fig. 4—Stress-strain curve for the simulated material obtained from torsion test (AA1100).^[26]

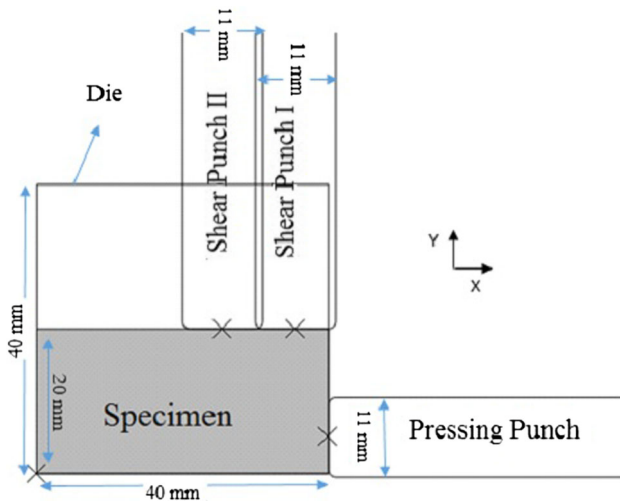


Fig. 3—Schematic representation of the simulated model.

tensor components were chosen to be history output. Then, the data were processed by Eq. [1] to calculate the strain rate tensor. It is worth to be mentioned that one element's strain history was chosen to be representative of its neighboring elements. This assumption seems reasonable for the elements that are located in some specified regions with close deformation history. The closeness of deformation history could be justified by

Table I. Elastic Properties Chosen for the Simulated Material

Material Name	Young Modulus (GPa)	Poisson Ratio
Aluminum 1100	70	0.33

monitoring and comparing the component of strain tensor throughout the whole straining time. In this study, these regions are named as shear zone and compression zone (see Section III). Similar methodology was used elsewhere.^[24] This approximated deformation history was used as an input to VPSC code^[8] provided by the Los Alamos National Laboratory. This code considers a rate sensitive constitutive relation to model material's behavior both in macroscopic and microscopic framework. To calculate strain in microscopic scale, this code assumes each grain as an inhomogeneity in homogenous medium and uses different linearization methods to relate stress and strain of this inhomogeneity to homogenous medium.

Initial random texture with 500 grain orientations was used to model texture evolution. Grain fragmentation and grain co-rotation schemes^[10] were used to capture grain refinement effects on texture evolution. Secant interaction type was used to model grain interaction with homogenous medium. FCC single crystal with voce-hardening type^[27] was used. Critical resolved shear stress of 1 MPa^[28,29] with no latent hardening effect^[30]

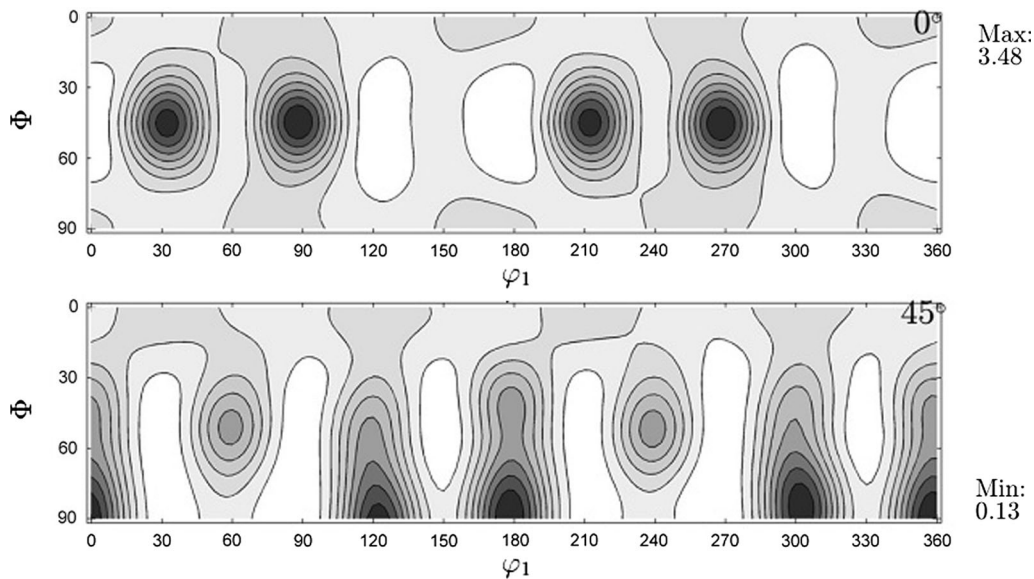


Fig. 5—The simple shear orientation distribution function produced by new methodology.

Table II. FCC Main Ideal Orientation in Simple Shear Mode of Deformation^[12]

Notation	$\{h\ k\ l\}\langle u\ v\ w\rangle$	Euler Angles (deg)		
		φ_1	ϕ	φ_2
A_1^*	$(111)[\bar{1}\bar{1}2]$	35.26/215.26	45	0/90
A_1^*	$(111)[11\bar{2}]$	125.26	90	45
A_1^*	$(111)[11\bar{2}]$	144.74	45	0/90
A_1^*	$(111)[11\bar{2}]$	54.74/234.74	90	45
A	$(\bar{1}\bar{1}1)[110]$	0	35.26	45
\bar{A}	$(\bar{1}\bar{1}1)[\bar{1}\bar{1}0]$	180	35.26	45
B	$(\bar{1}\bar{1}2)[110]$	0/120/240	54.74	45
\bar{B}	$(111)[11\bar{2}]$	60/180	54.74	45
C	$\{001\}\langle 110\rangle$	90/270	45	0/90
C	$\{001\}\langle 110\rangle$	0/180	90	45

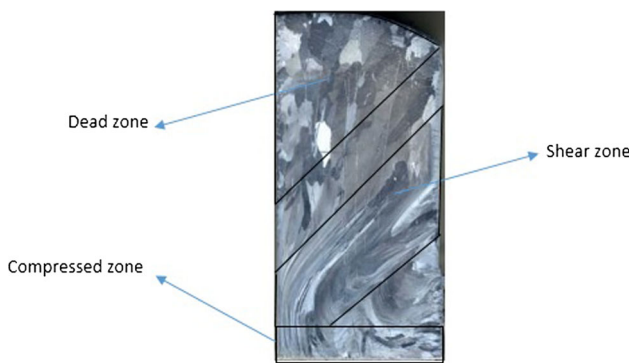


Fig. 6—Macro-etched aluminum after one pass of MAIFS.

was assumed. Rate sensitivity exponent in visco-plastic constitutive equation was assumed to be equal to 20.^[28]

After processing deformation history by VPSC code, ODF data were post processed by Mtex texture analyzer software^[31] to analyze texture evolution in the MAIFS process. Calculated texture evolution in different parts

of specimen was then compared to simple shear texture case.

C. Verification of Methodology

In order to validate the applied methodology, results of simulations based on the proposed method were compared with the reported results^[12] for simple shear case as shown in Figure 5. The analysis reproduces the components of ideal simple shear that is indicated by Table II.

These results are in the best possible agreement with the literature^[5-7] and they are comparable with the experimental results reported for processes that are dealt with simple shear mode of deformation (e.g., ECAE^[32]). Therefore, it can be said that the present methodology is capable of tracing all texture components that are evolved in a specified deformation history.

Since the methodology gives the reasonable results for simple shear case, it can be anticipated that application of this procedure will lead to acceptable results for the other deformation conditions.

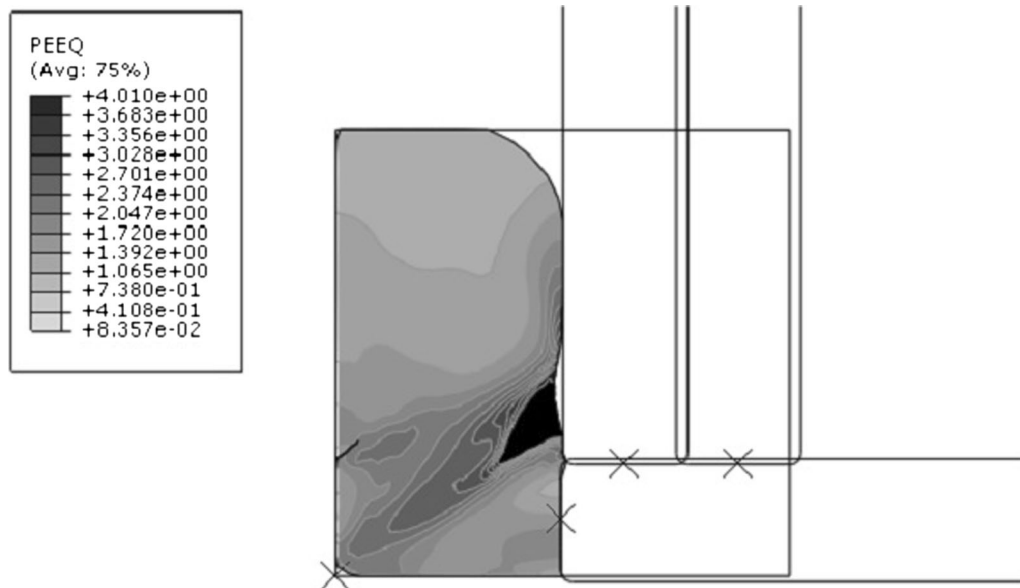


Fig. 7—Distribution of equivalent strain in deformed part after simulation.

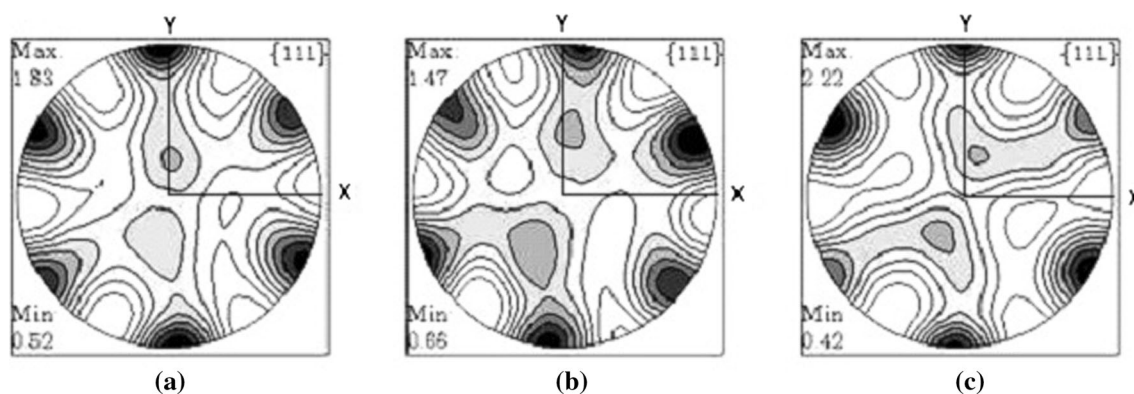


Fig. 8—(1 1 1) pole figures simulated from (a) compressed zone, (b) shear band zone, (c) simple shear. The black color shows the maximum intensity and the white shows the minimum.

III. RESULTS AND DISCUSSION

Figure 6 shows the macro-etched section of deformed 1100 aluminum specimen. As can be seen in this figure, after first pass of the MAIFS process, a large inhomogeneity has been developed in the aluminum specimen. Four distinct zones can be determined in the specimen: compressed zone, shear zone, transition zone, and dead zone. These deformation zones configurations are in good agreement with finite element simulation results as shown in Figure 7. Due to accordance with experimental and simulation results, it is sufficient to have an insight in shear zone and compressed zone for investigating texture evolution in the MAIFS process.

Figure 8 represents (1 1 1) pole figures for the compressed zone (Figure 7(a)) and shear band zone (Figure 7(b)). Simple shear's (1 1 1) pole figure was also included in this figure as (Figure 7(c)) for sake of comparison. Comparison of Figures 7(a) and 7(b) qualitatively shows that the simple shear-like (1 1 1)

pole figure was developed in both compressed and shear deformation zones and just the maximum intensity is reduced and ideal orientations are slightly rotated in pole figures in comparison to the simple shear case.

Figure 9 and Table II represent the ideal orientation in FCC polycrystal which experienced simple shear mode of deformation from finding of Li *et al.*^[12] These ideal orientations as well as developed orientations in 0 and 45 deg sections of shear and compressed zones of MAIFS process are also shown in Figure 11. Figure 8 qualitatively shows that the same ideal orientation in simple shear was developed in the compressed area. ODF analysis in Figure 11 shows that main orientations in simple shear coincide with the main orientations of compressed zone but with a very slight rotation. The same analysis for shear zone shows that in comparison to simple shear, different partial fibers were developed in shear zone. There is also large rotation in texture component of this zone. This observation can be

attributed to the more complex mode of deformation in this zone. The term “complex mode of deformation” can be more specifically addressed by displacement gradient, (Δk of Reference 30). The displacement

gradient is composed of rigid body rotation increment and strain increment tensor. More details on its formulation and concept can be found elsewhere.^[33] Two shear planes exist in x - y plane of shear zone: One between first and second shear punches shown in Figure 3 and the other shear plane exists in the final non-equal channel (Figure 10 shows these two shear planes). The differences in shear planes angles to the horizontal direction lead to rotation in (1 1 1) pole figure presented in Figure 8(b) and rotation in ODF space (Figure 11). These results show the importance of components of deformation other than main shear component in texture evolution.

Another important observation in pole figures presented in Figure 8 is the maximum intensity and distribution of orientations. In the MAIFS process, the maximum determined intensity for all of the studied zones is less than that evaluated intensity for the simple shear case. These phenomena can be related to the more complexity of the deformation in the studied zones compared to simple shear one. In shear zone, other components of strain tensor beside the shear components are active. These components change as deformation develops (there exist three steps of deformation with a three different deformation history). As more strain components are activated, there is more chance for activation of more crystalline slip planes. Figure 12 shows the average activated slip planes in the MAIFS and simple shear processes. As can be observed, in the MAIFS process, there is always more activated slip plane than the simple shear process and this leads to more randomization in final texture. This phenomenon is important for encouraging homogeneity and development of the ultra-fine grain structure in the final product of MAIFS after several passes. This shows that

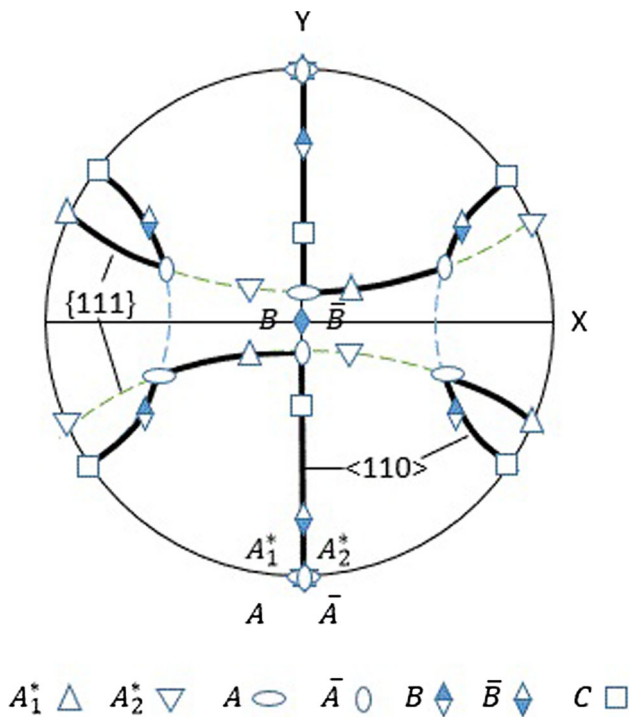


Fig. 9—Key figure for ideal orientation poles on pole figure analysis obtained and reproduced from Ref. [12].

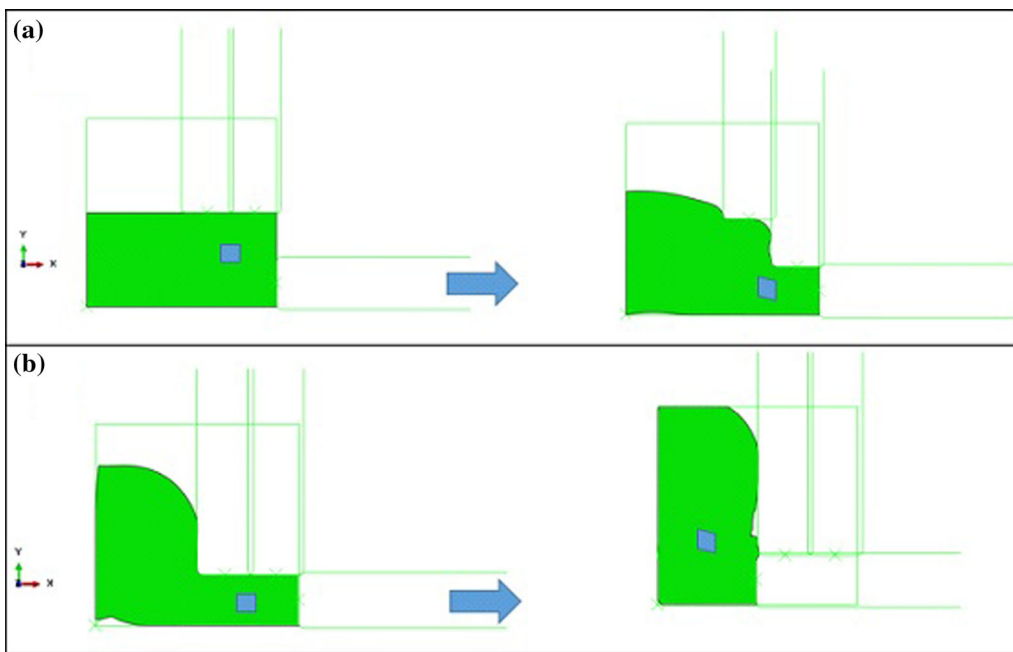


Fig. 10—Two shear planes that exist in the process (a) in second step and (b) Final step.

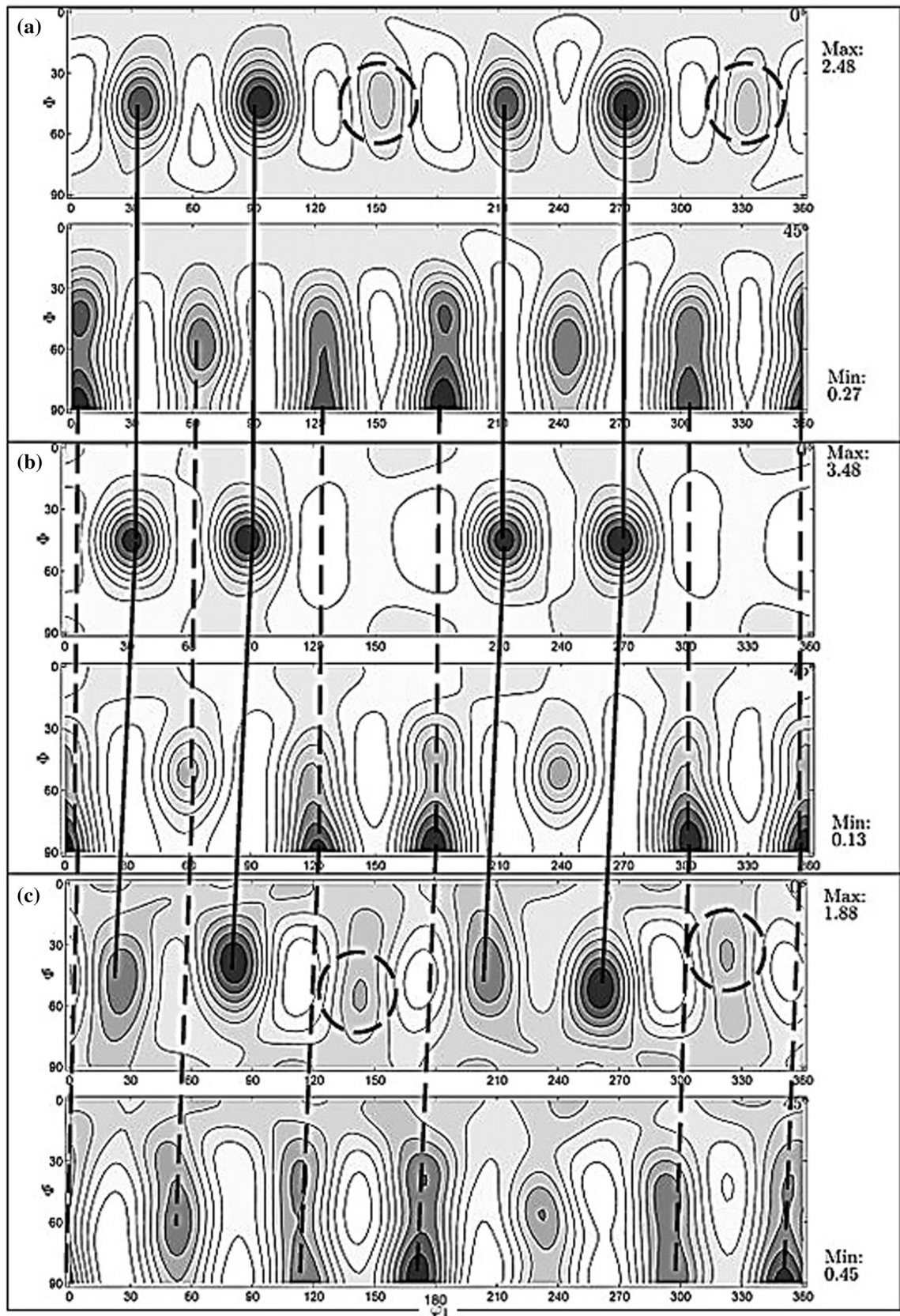


Fig. 11—ODF texture representation in 0 and 45 sections for (a) compressed zone (b) simple shear (c) shear zone. Circles show the new partial fibers. Solid lines and dashed lines are used to show rotation in 0 and 45 sections, respectively.

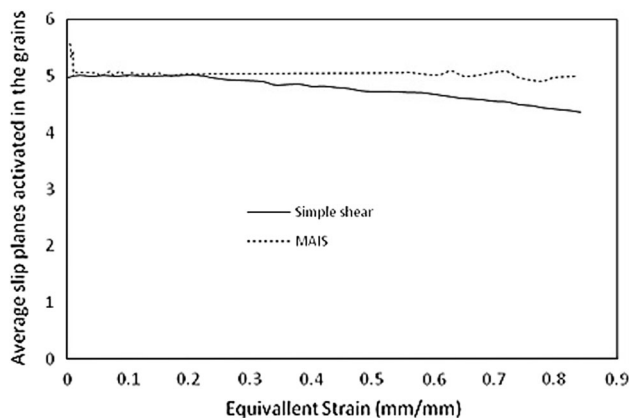


Fig. 12—Average slip planes activated in MAIFS and simple shear deformation.

the grain refinement efficiency can be enhanced in the MAIFS process compared to the simple shear processes.

IV. CONCLUSIONS

In this paper, after finite element simulation of one newly developed SPD named MAIFS, VPSC analysis was conducted to learn more about texture evolution in this process. After the analysis and comparison of result with simple shear simulation, it can be concluded that

1. Although simple shear-like textures develop in two severely deformed zones, there are considerable differences in texture patterns.
2. In compressed zone, texture component is similar to the simple shear texture with slight rotation around normal direction to x - y plane.
3. In shear band zone, texture components are weaker than the simple shear texture component and a large rotation in texture component can be observed in the final pole figure. This rotation is related to the complexity in the deformation mode, where non-shear type components of deformation affect this rotation.
4. In all observed pole figures, the intensities for the MAIFS process are lower than those observed for the simple shear deformation. This behavior is related to high chance of more activated slip planes in deformation history. This behavior is important because the efficiency in grain refinement could be improved by this process. It can be concluded that if more shear punches would be used, the more grain refinement efficiency can be obtained.

REFERENCES

1. R.Z. Valiev, R.K. Islamgaliev, and I.V. Alexandrov: *Prog. Mater. Sci.*, 2000, vol. 45, pp. 103–89.
2. L.S. Toth and C. Gu: *Mater. Charact.*, 2014, vol. 92, pp. 1–14.
3. V.M. Segal: *Mater. Sci. Eng. A*, 1999, vol. 271, pp. 322–33.
4. Y. Estrin and A. Vinogradov: *Acta Mater.*, 2013, vol. 61, pp. 782–817.
5. A. Gholinia, P. Bate, and P. Prangnell: *Acta Mater.*, 2002, vol. 50, pp. 2121–36.
6. L.S. Tóth: *Adv. Eng. Mater.*, 2003, vol. 5, pp. 308–16.
7. L.S. Tóth, R. Arruffat Massion, L. Germain, S.C. Baik, and S. Suwas: *Acta Mater.*, 2004, vol. 52, pp. 1885–98.
8. R. Lebensohn and C. Tomé: *Acta Metall. Mater.*, 1993, vol. 41, pp. 2611–24.
9. G.Y. Deng, C. Lu, L.H. Su, J.T. Li, H.T. Zhu, X.H. Liu, and K. Tieu: *Adv. Mater. Res.*, 2013, vol. 651, pp. 442–47.
10. I. Beyerlein, R. Lebensohn, and C. Tome: *Mater. Sci.*, 2003, vol. 345, pp. 122–38.
11. S. Ferrasse, V. Segal, S. Kalidindi, and F. Alford: *Mater. Sci. Eng. A*, 2004, vol. 368, pp. 28–40.
12. S. Li, I.J. Beyerlein, and M.A.M. Bourke: *Mater. Sci. Eng. A*, 2005, vol. 394, pp. 66–77.
13. S. Li, S.R. Kalidindi, and I.J. Beyerlein: *Mater. Sci. Eng. A*, 2005, vols. 410–411, pp. 207–12.
14. I.V. Alexandrov, M.V. Zhilina, A.V. Scherbakov, A. Korshunov, P.N. Nizovtsev, A.A. Smolyakov, V.P. Solovyev, and I.J. Beyerlein: *Mater. Sci. Forum*, 2005, vols. 495–497, pp. 785–90.
15. S.R. Kalidindi, B.R. Donohue, and S. Li: *Int. J. Plast.*, 2009, vol. 25, pp. 768–79.
16. G.Y. Deng, C. Lu, L.H. Su, A.K. Tieu, H.L. Yu, and X.H. Liu: *Comput. Mater. Sci.*, 2013, vol. 74, pp. 75–85.
17. C. Lu, G.Y. Deng, A.K. Tieu, L.H. Su, H.T. Zhu, and X.H. Liu: *Acta Mater.*, 2011, vol. 59, pp. 3581–92.
18. I.J. Beyerlein and C.N. Tomé: *Mater. Sci. Eng. A*, 2004, vol. 380, pp. 171–90.
19. J. Rossiter, A. Brahme, M.H. Simha, K. Inal, and R. Mishra: *Int. J. Plast.*, 2010, vol. 26, pp. 1702–25.
20. D.D. Tjahjanto, P. Eisenlohr, and F. Roters: *Model. Simul. Mater. Sci. Eng.*, 2010, vol. 18, pp. 015006(21).
21. Y. Aoyagi, R. Kobayashi, Y. Kaji, and K. Shizawa: *Int. J. Plast.*, 2013, vol. 47, pp. 13–28.
22. A. Ostapovets, P. Šedá, A. Jäger, and P. Lejček: *Int. J. Plast.*, 2012, vol. 29, pp. 1–12.
23. J. Segurado, R.A. Lebensohn, J.L. Lorca, and C.N. Tomé: *Int. J. Plast.*, 2012, vol. 28, pp. 124–40.
24. M. Montazeri-Pour and M. Habibi-Parsa: *Adv. Mater. Res.*, 2014, vol. 829, pp. 15–19.
25. G.F. Voort, Vander: *Metallography and Microstructures*, ASM International Materials Park, 2006, pp. 1061–62.
26. S. Li, M.A.M. Bourke, I.J. Beyerlein, D.J. Alexander, and B. Clausen: *Mater. Sci. Eng. A*, 2004, vol. 382, pp. 217–36.
27. C. Tome, G. Canova, and U. Kocks: *Acta Metall.*, 1984, vol. 32, pp. 1637–53.
28. C. Tomé and R. Lebensohn: Manual for code viscoplastic self-consistent (version 7), Los Alamos Natl. Lab., 2009, pp. 1–110.
29. G.E. Totten and D.S. MacKenzie: *Handbook of Aluminium: Physical Metallurgy and Processes*, vol. 1, CRC, New York, 2003, p. 212.
30. W. Mingzhang, L. Shi, L. Chenghua, W. Zhongguang, and X. Jimei: *Scripta Mater.*, 1996, vol. 35, pp. 1183–88.
31. F. Bachmann, R. Hielscher, and H. Schaeben: *Solid State Phenom.*, 2010, vol. 160, pp. 63–68.
32. S. Suwas, R.A. Massion, L.S. Tóth, J.-J. Fundenberger, and B. Beausir: *Mater. Sci. Eng. A*, 2009, vol. 520, pp. 134–46.
33. X. Hu, G.A. Cingara, D.S. Wilkinson, M. Jain, P. Wu, and R.K. Mishra: *Comput. Mater. Contin.*, 2010, vol. 14, pp. 99–124.